Int J Clin Exp Med 2017;10(2):2992-3004
www.ijcem.com /ISSN:1940-5901/IJCEM0041735

Original Article

Imaging features of intrahepatic mass-forming cholangiocarcinomas on Gd-BOPTA-enhanced MRI

Lin Yang[1], Zhihong Shi[1], Ying Zhang[2], Zhiling Liu[1], Zhaoqin Huang[1], Yinghui Xin[1], Lei Bi[1], Xue Han[3], Jianjun Xiu[1]

Departments of [1]Radiology, [3]Ultrasonic Diagnosis and Treatment, Shandong Provincial Hospital Affiliated to Shandong University, Jinan, China; [2]Department of Radiology, Shandong Heze Municiple Hospital, Heze, China

Received October 12, 2016; Accepted November 16, 2016; Epub February 15, 2017; Published February 28, 2017

Abstract: Objective: The purpose is to describe the imaging features of intrahepatic mass-forming cholangiogcarcinoma (IMC) with emphasis on hepatobiliary phase (HBP) on Gd-BOPTA-enhanced MR imaging. Methods: We retrospectively reviewed 93 patients with pathologically proven IMCs with MR hepatocyte-specific contrast agent Gd-BOPOTA. We evaluated the enhancement pattern, degree of enhancement and conspicuity of IMCs. We also analyzed diffusion-weighted (DW) images and measured the apparent diffusion coefficient (ADC) values of IMCs. Results: 80 (86.0%) lesions exhibited peripheral enhancement in arterial phase followed by progressive enhancement in portal venous and delayed phases. On HBP, 85 (91.4%) lesions exhibited peripheral hypointensity with central hyperintensity. On HBP, IMCs exhibited the highest conspicuities, and the degrees of enhancement were higher in moderately differentiated tumors (48.2% ± 15.6%) than in poorly differentiated tumors (35.5% ± 18.9%) and in the lesions without lymph node metastasis (47.6% ± 18.8%) than with lymph node metastasis (33.7% ± 19.6%). Additionally, the ADCs of poorly differentiated tumors were lower than those of moderately differentiated tumors. Conclusion: The typical pattern of IMCs on Gd-BOPTA-enhanced images HBP images was peripheral hypointensity with central hyperintensity. IMCs exhibited better delineation on HBP images, and the ADCs of poorly differentiated IMCs were lower, which may aid reasonable surgical planning and improve prognoses.

Keywords: Cholangiocarcinoma, Gd-BOPTA, liver hepatobiliary, MR, DWI

Introduction

Cholangiocarcinoma is the second-most common primary tumor of the liver following hepatocellular carcinoma (HCC) and accounts for 15%-20% of hepatic malignant tumors. The incidence of cholangiocarcinoma has gradually increased in recent years around the world [1, 2]. Cholangiocarcinoma originates in the epithelia of bile ducts [3], and intrahepatic cholangiocarcinoma accounts for 5%-10% of these lesions [4]. According to the growth patterns and morphologies, intrahepatic cholangiocarcinoma can be divided into the following three types: mass-forming, periductal infiltrating, and intraductal growth [5]. Intrahepatic mass-forming cholangiocarcinoma (IMC) accounts for 60% of intrahepatic cholangiocarcinoma [5]. Due to the poor prognoses of IMC, surgical resection is the only viable treatment [5], and the correct diagnoses of IMC are important for optimizing treatment plans and improving patient prognoses.

The development of imaging technology has enabled the use of ultrasound (US), computerized tomography (CT) and magnetic resonance (MR) imaging for the diagnoses of IMC [6]. MR is considered the clinical reference standard for detecting and characterizing liver focal lesions due to its intrinsically excellent soft-tissue contrast and superior sensitivity [7]. For many years, conventional extracellular contrast material was routinely used in liver MR imaging [8, 9]. In recent years, hepatocyte-specific contrast agents has been used in liver MR. Because these agents have the properties of both traditional contrast agents and liver-specific contrast agents [10], they can be used in MR scans as hepatocyte-specific contrast agents and enable the acquisition of images in both the dynamic enhancement phase and hepatobiliary

Table 1. Main patient characteristics

Number of patients	93
Mean age ± standard deviation (years)	63.5 ± 11.6
Age range (years)	42-78
Sex Male/Famle (number, %)	68 (73.1%)/25 (26.9%)
Number of patients with chronic hepatitis	17 (hepatitis B, 15; hepatitis C, 2)
Mean age of male patients ± standard deviation (years)	59 ± 13.5
Age range of male patients (years)	42-78
Mean age of female patients ± standard deviation (years)	64 ± 10.8
Age range of female patients (years)	56-75
Lesion location (number, %)	
Left	57 (61.3%)
Right	26 (28.0%)
Central	10 (10.7%)
Lesion diameter mean (cm) ± standard deviation	6.2 ± 2.5
Lesion diameter range (cm)	2.2-12.3

phase (HBP). Gd-BOPTA and Gd-EOB-DTPA are the two most common liver-specific contrast agents. Compared to other extracellular contrast agents, hepatocyte-specific contrast agents provide excellent images in liver MR during the dynamic phases due to increased relaxivity [11], and contrast agents can be taken up by functional hepatocytes and excreted into the bile due to the hepatobiliary properties of HBP [12, 13]. In our study, we observed the imaging features of IMC on Gd-BOPTA-enhanced MR imaging. Gd-BOPTA was selected for our study rather than Gd-EOB-DTPA. Although Gd-BOPTA exhibits a later hepatobiliary phase (90-120 min) and a lower biliary excretion (3%-5%) [14], it is less expensive, provides a greater degree of vessel enhancement, and provides a comparable enhancement of the liver parenchyma [13].

Materials and methods

Patient selection

We searched the electronic medical records of hospital and revealed that there were 185 patients with the diagnosis of IMCC who had visited our hospital between January 2009 and December 2015. Finally, we selected 93 patients who exactly met the following criteria: (a) all of the lesions in the patients were treated with surgical resection and pathologically confirmed to be cholangiocarcinomas (40 patients were excluded); (b) the patients all underwent the MR standard protocol described below, and the MR images were sufficiently clear and free of motion artifacts for use in the imaging analyses (11 patients were excluded); (c) the patients did not undergo MR examintions with non-speciic extracellular contrast materials in a short period of time (one month) (6 patients were excluded); and (d) the patients did not have histories of treatments including transcatheter arterial chemoemboliztion, radiofrequency ablation, or percutaneous ethanol injection prior to the MR examinations (14 patients were excluded). Additionally, the cholangiocarcinomas of 21 patients were proven without surgery and with percutaneous biopsy, considering the limitations of biopsy, it is likely that combined hepatocellular and cholangiocarcinomas (HCC-CC) were mistaken for cholangiocarcinomas, thus, we excluded the 21 patients from this study for this reason. The patient details are displayed in **Table 1**. This study was approved by the ethics board of our institution.

MR protocol

All imaging was performed on a 3.0 T MRI system (Magnetom Verio, Siemens, Germany). All patients were imaged in the supine head-first position with a surface phased array coil. Breath-hold transverse T2-weighted turbo spin-echo sequences (repetition time [TR] 3000-4000 ms and echo time [TE] 90-104 ms) were initially performed and followed by transverse T1-weighted dual-echo in-phase and out-of-phase sequences (flip angle, 70°; TR, 130; TE, 2.3 ms in-phase; TE, 3.7 ms out-of-phase) with a 5-mm slice thickness and a 1-mm interspace. Three-dimensional fat-saturated T1-weighted

dynamic contrast-enhanced sequences (volume interpolated body examination, Siemens, Germany) were applied during suspended respiration. Gadobenate dimeglumine (Gd-BOPTA, MultiHance, 0.1 mmol/kg) was injected intravenously as a contrast agent at a rate of 2.5 ml/s via a power injector and followed with a 20-mL saline flush. Dynamic contrast-enhanced MRI was performed in the transverse plane with a 3-mm slice thickness in the hepatic arterial phase (20-25 s), portal venous phase (60-70 s), delayed phase (5 min), and hepatobiliary phase (HBP) (90-100 min) following contrast injection.

Before the dynamic contrast-enhanced imaging, a transverse respiratory-triggered DW single-shot echo-planar imaging (SS-EPI) sequence was applied with tri-directional diffusion gradients using two b values of 0 and 800 sec/mm^2. ADC maps were generated with a commercially available software workstation system (Syngo Multimodality workplace, Siemens, Germany).

Image analysis

All of the magnetic resonance images were reviewed by two radiologists on a picture archiving and communication system workstation (PACS, GE Healthcare, USA). The two radiologists had 20 and 8 years of diagnostic experience in abdominal imaging, respectively, and this was an independent review by each reviewer. The radiologists knew that the reviewed lesions were cholangiocarcinomas but were blind to all additional histopathological details. The MR images were reviewed in a random order to avoid bias. Disagreements were resolved based on the views of the third radiologist (12 years of experience in abdominal imaging) until consensus was achieved. We evaluated 93 lesions in 93 patients, and no distant metastases were found in the hepatic segments outside of the lesions. In cases in which small nodules (defined as satellite nodules) were present around the lesion within the same hepatic segment, we evaluated only the dominant mass.

Qualitative analysis

We analyzed the signal intensities (SIs) of the lesions on unenhanced T1WI and T2WI images relative to the adjacent normal liver parenchyma. The SI was recorded as follows: (a) homogeneous hyperintense, (b) inhomogeneous hyperintense, (c) homogeneous hypointense, (d) inhomogeneous hypointense, and (e) isointense. Hyperintensity was defined as a relative SI of the lesion that exceeded the adjacent normal liver parenchyma, hypointensity was defined as a lesion SI below that of the adjacent normal liver parenchyma, and isointensity was defined as a lesion SI equal to that of the adjacent normal liver parenchyma.

We evaluated the signal intensity in the center and periphery of each lesion relative to the intensity of the adjacent normal parenchyma in the arterial phase, portal venous phase, delayed phase and hepatobiliary phase (HBP). According to the signal characteristics, we recorded the lesions as within the following categories: (a) homogeneous hyperintensity, (b) inhomogeneous hyperintensity, (c) homogeneous hypointensity, (d) inhomogeneous hypointensity, (e) central hyperintensity with peripheral hypointensity, (f) central hypointensity with peripheral hyperintensity, (g) central hypointensity with lower peripheral lower rim hypointensity, and (h) central hyperintensity with higher peripheral rim hyperintensity. We also recorded the signal characteristics of the IMC on diffusion-weighted (DW) images according to their performances.

We evaluated the enhancement patterns of each of the lesions and recorded these patterns as follows: (a) progressive enhancement: peripheral enhancement in the arterial phase and progressive centripetal enhancement in the portal venous phase and delayed phase; (b) weak enhancement in the arterial phase followed by gradual enhancement in portal venous and delayed phases. We defined weak enhancement as that the lesion SI was lower than the normal liver parenchyma SI on MR enhancement images. (c) wash in with wash out: strong enhancement in the arterial phase and washing out in the portal venous and delayed phases; (d) no enhancement; and (e) stable: enhancement that was nearly invariant throughout the arterial, portal venous and delayed phases.

Based on the heterogeneity of the internal structures of the lesions, we defined hyperintensity on T2WI images combined with low SI on T1WI images and the lack of enhancement on the post-enhancement images as liquefaction and necrosis, respectively. We also record lesion morphologic changes as (a) bile duct

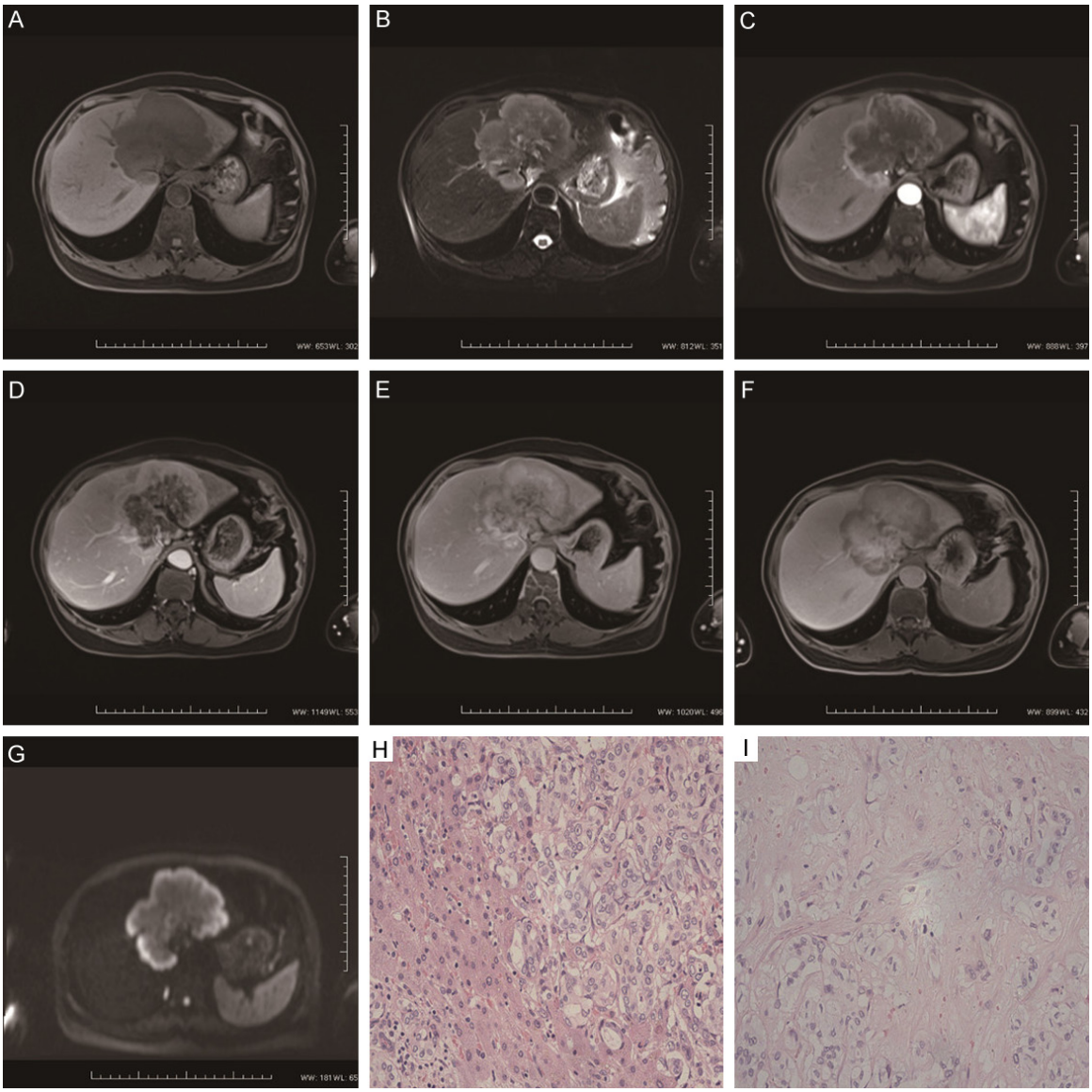

Figure 1. A 65-year-old woman with a histologically proven moderately differentiated intrahepatic mass-forming cholangiocarcinoma. The lesion exhibits inhomogeneous hypointensity on T1WI 3D GRE with fat-saturation (A) and inhomogeneous hyperintensity on T2WI FSE with fat-saturation (B) compared with the adjacent liver parenchyma. Following the injection of Gd-BOPTA, the tumor exhibited peripheral rim enhancement in the arterial phase (C) and progressive centripetal enhancement in the portal venous phase (D) and 10-min delayed phase (E). On HBP (F), the lesion exhibited periphery rim-like hypointensity with central hyperintensity. In the delayed phase (E) and HBP (F), the appearance of the target was observable. An axial DW image (G) (b value of 800 sec/mm^2) also revealed the appearance of the target with the performance of the peripheral rim hyperintensity with central hypointensity. Photograph (H) is a microscopic image of the periphery of the tumor (H&E, ×400), it revealed a large number of tumor cells and plentiful tumor vessels in the periphery. Photograph (I) shows a microscopic image of the center of the tumor (H&E 400) and indicated that the majority of the fibrous tissue was the center.

dilation, (b) adjacent liver capsule retraction, (c) the adjacent liver capsule retraction or bulging, (d) satellite nodules, (e) lymph node metastases, (f) vascular invasion.

In order to study which MR sequences can provide the best conspicuity and border of IMCs in dynamic phase and HBP images, we rated the borders of IMCs compared to adjacent liver tissues as 1= ill-defined, 2= blurred border, 3= moderately border, 4= sharp border, 5= well-defined. We also observed which sequences the satellite nodules can be found in dynamic phase and HBP images.

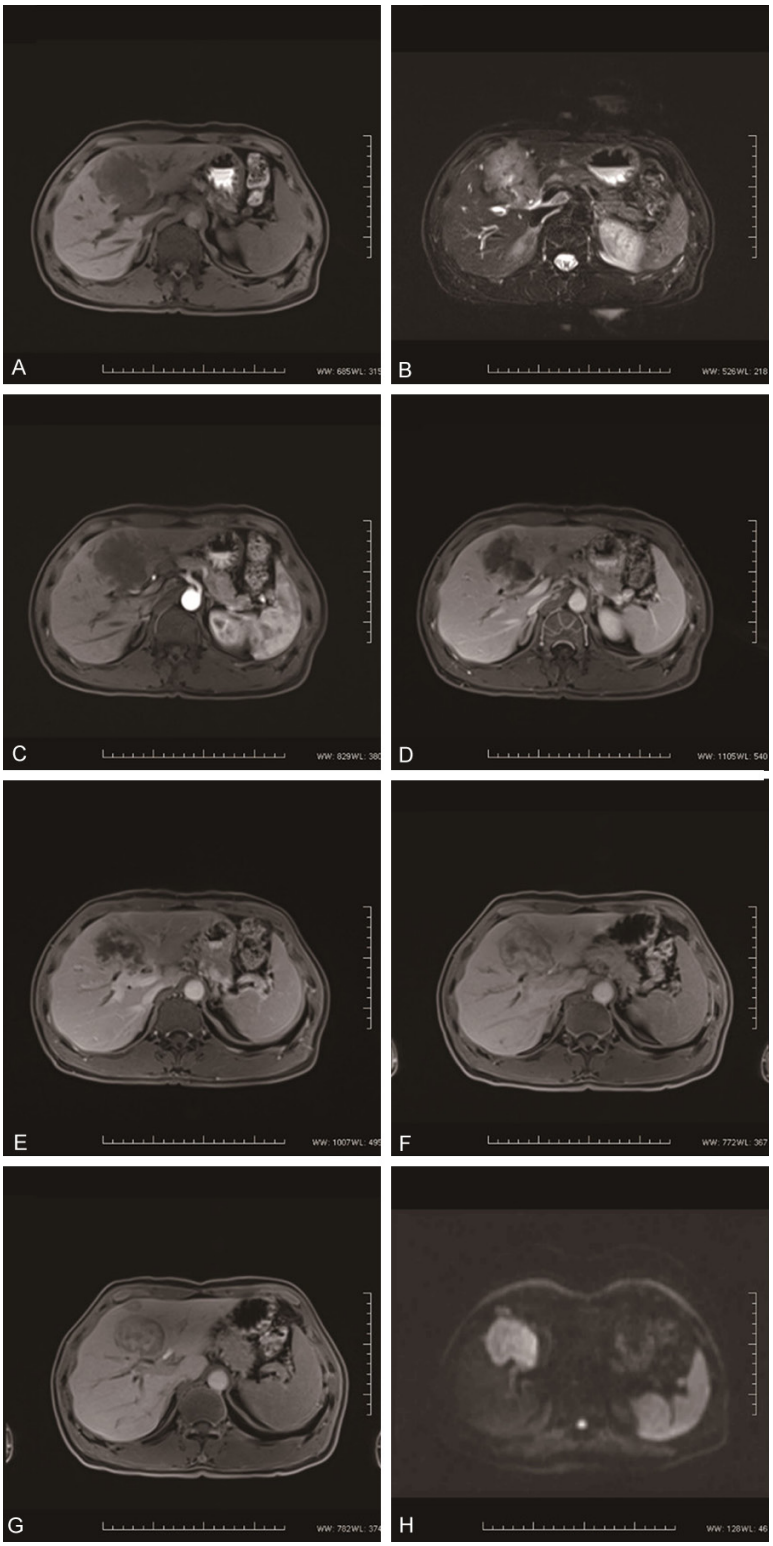

Figure 2. A 73-year-old man with a histologically proven poorly differentiated intrahepatic mass-forming cholangiocarcinoma. The lesion exhibits an inhomogeneous hypointensity on T1WI 3D GRE with fs (A) and a inhomogeneous hyperintensity on T2WI FSE with fs (B) compared to the adjacent liver parenchyma. Following the injection of Gd-BOPTA, the tumor exhibited weak peripheral rim enhancement in the arterial phase (C) and gradual enhancement in the portal venous phase (D) and delayed phase (E). On HBP (F, G), the exhibited a periphery rim-like hypointensity with a central hyperintensity. In the delayed phase (E), the HBP (F, G) and DW (H) images revealed that the target could be observed. The satellite nodule can be more clearly observed in the HBP phases (F, G).

Quantitative analysis

We used regions of interest (ROI) to measure the SIs in the pre-enhancement images and the arterial, portal venous, delayed and hepatobiliary phase images. The lesion ROI was made as large as possible (The ROI ranged from 39.5-5878.9 mm^2). The normal liver parenchyma ROI were placed in the same slices as the lesions. The ROI measurement avoided large blood vessels, necrosis and artifacts. All SIs of the ROI were measured twice, and the average of these measurements were used. Moreover, we calculated the relative contrast enhancement percentages of the lesions and the adjacent normal liver parenchyma in the post-enhancement phase with the following formula: (SIpost-SIpre)/SIpre ×100% [15]. We measured the ADC values of all of the lesions. The ROIs on the ADC maps was made as large as possible in the solid part of the lesions and also avoided areas of necrosis and cystic degeneration. Within the same slices, we also calculated the ADC values of the adjacent normal parenchyma. The ADC values were also measured twice, and the averages of these values were used. All of the above measurements and calculations

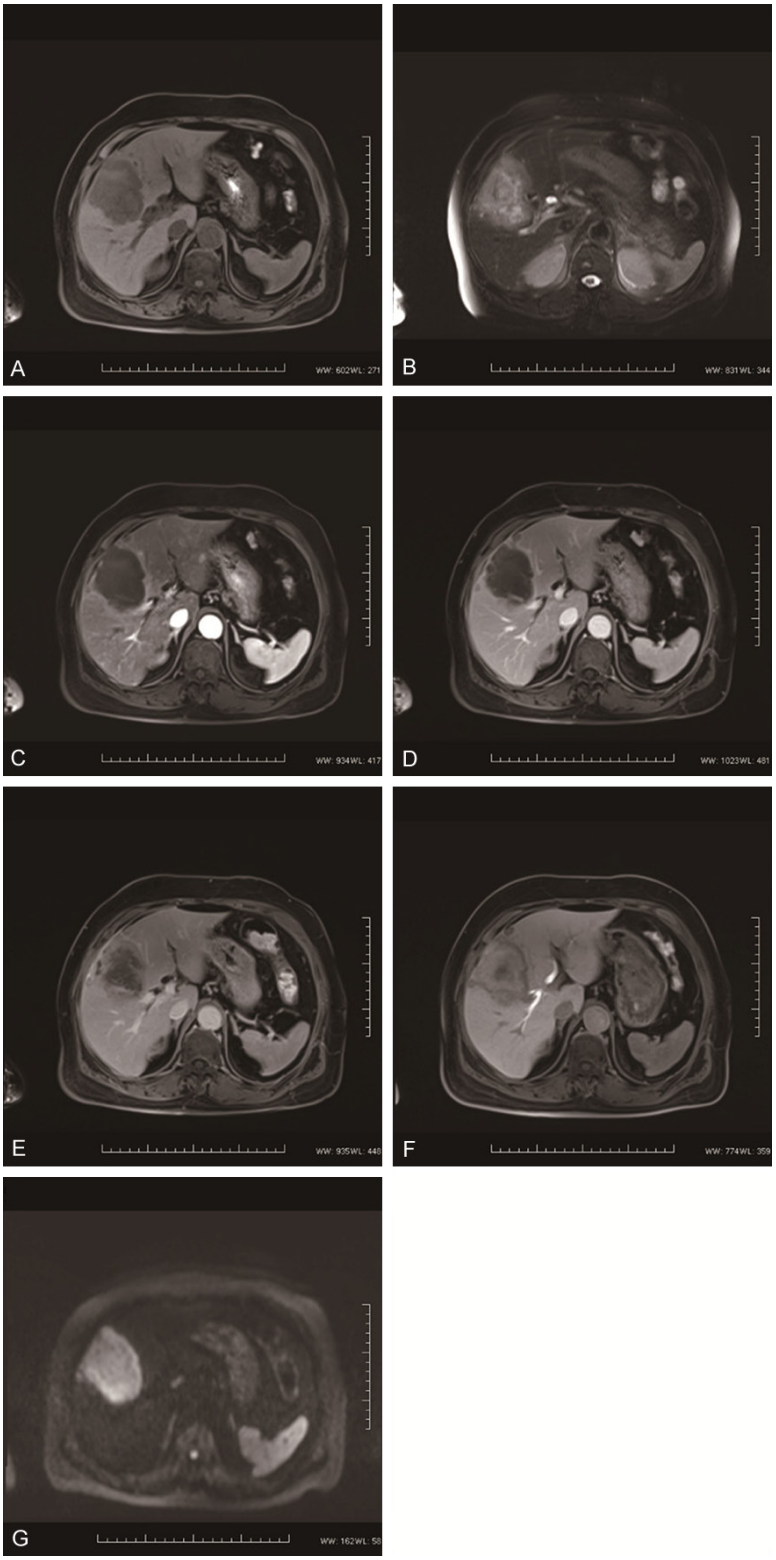

Figure 3. A 69-year-old man with a histolocally proven poorly different-ated intrahepatic mass-forming cholangiocarcinoma. The lesion exhibited inhomogeneous hypoitensity on T1WI (A) and inhomogeneous hyperintensity on T2WI (B). After the injection of Gd-BOPTA, the tumor exhibited a peripheral rim enhancement in the arterial phase (C), and a gradual enhancement in the portal venous phase (D) and delayed phase (E). On HBP (F), the lesion exhibited a periphery rim-like hypointensity with a central hyperintensity. The areas of central hypointensity exhibited in the delayed phase were almost completely overlapped by hyperintensity in on HBP (F). In the delayed phase (E), the target appearance can be observed on the HBP (F) and DW images (G). The tumor and satellite nodule borders are be more clearly depicted on the HBP (F). Strong enhancement of the intrahepetic bile duct can be observed on the HBP (F), which may indicate normal liver function in the patient.

were completed by a single radiologist with six years of abdominal imaging experience.

Additionally, to further study the characteristics of the lesions on HBP images and ADC maps, we divided the lesions into six subgroups based on the following morphological and histopathological characteristics: 1, the degree of differentiation; 2, the presence or absence of lymph node metastasis; 3, the presence or absence of satellite nodules; 4, the presence or absence of bile duct invasion; 5, the presence or absence of serosal invasion; and 6, the presence or absence of vascular invasion. We compared the degrees of enhancement on the HBP images and the ADCs of the lesions of the six subgroups.

Statistical analysis

All statistical analyses were performed using SPSS version 17.0 for Windows. In the qualitative analysis, the interobserver agreements regarding the enhancement patterns and the signal intensities were evaluated with κ statistics. We used the κ val-

Table 2. Signal characteristics of IMCs in each phase and DW images

	Arterial phase	Portal vein phase	Delayed phase	HBP	DWI
Central hypointensity with peripheral hyperintensity	80 (86.0%)	65 (69.9%)	0	0	34 (36.6%)
Central hyperintensity with peripheral hypointensity	0	25 (26.9%)	70 (75.3%)	86 (92.5%)	0
Central hypointensity with peripheral rim hypointensity	0	0	21 (22.6%)	0	0
Central mixed signals with peripheral hyperintensity	0	0	0	0	47 (50.5%)
Inhomogeneous hypointensity	11 (11.8%)	1 (1.1%)	1 (1.1%)	6 (6.5%)	0
Inhomogeneous hyperintensity	1 (1.1%)	0	0	0	13 (14.0%)
High-low mixed signal intensity	0	0	0	1 (1.1%)	0

Table 3. Degree of enhancement of IMC on HBP images and ADCs of IMC

Morphologic and histopathological characteristics	Number of patients	Mean degree of enhancement (%)*	*P* value	Mean ADCs (10^{-3} mm^2/s)*	*P* value
Differentiation					
Moderate	38	48.2 ± 15.6	0.028	0.98 ± 0.22	0.033
Poor	55	35.5 ± 18.9		0.75 ± 0.18	
Lymph node metastasis					
Present	21	33.7 ± 19.6	0.022	0.78 ± 0.31	0.875
Absent	72	47.6 ± 18.8		0.89 ± 0.41	
Satellite nodule					
Present	39	46.3 ± 28.8	0.059	0.75 ± 0.19	0.088
Absent	54	48.9 ± 14.2		0.91 ± 0.24	
Bile duct invasion					
Present	44	39.6 ± 17.2	0.445	0.87 ± 0.11	0.909
Absent	49	44.5 ± 13.6		0.89 ± 0.24	
Serosal invasion					
Present	36	45.8 ± 22.5	0.874	0.76 ± 0.78	0.669
Absent	57	42.7 ± 18.6		0.87 ± 0.24	
Vascular invasion					
Present	23	36.8 ± 18.6	0.589	0.81 ± 0.35	0.671
Absent	70	42.6 ± 14.2		0.84 ± 0.28	

*Data of Degree of Enhancement and ADC are mean standard ± deviation (x ± SD).

ues to measure the degrees of interobserver agreement as follows [16]: 0.81≤κ≤1.00, excellent agreement; 0.61≤κ≤0.80, substantial agreement; 0.41≤κ≤0.60, moderate agreement; 0.21≤κ≤0.40, fair agreement; and κ≤0.20, slight agreement. We used Wilcoxon signed-rank tests to evaluate the conspicuities of the lesions on the dynamic phase and HBP images. For the quantitative analysis, all of the data we measured are expressed as the means ± the standard deviations (x ± SD). For the comparisons of the percentages of enhancement of the lesions on the HBP images and the comparisons of the ADCs between the subgroups, we used two-tailed unpaired Student's t tests. *P* values below 0.05 were considered significant.

Results

Results of the qualitative analyses

Interobserver agreement: Regarding the evaluations of the relative signal intensities of the lesions in each phase, the interobserver agreement was excellent (κ=0.838). Regarding the assessments of the lesion enhancement patterns, interobserver agreement was also excellent (κ=0.902).

Signal characteristics of the lesions in each sequence and enhancement phase

The SI on the pre-enhancement and post-enhancement images were evaluated. All of

the lesions exhibited homogeneous or inhomogeneous hypointense on the T1WI images and homogeneous or inhomogeneous hyperintense on the T2WI compared with the adjacent liver parenchyma.

In the post-enhancement images, the majority of the lesions (86.0%, 80) exhibited central hypointensity with peripheral hyperintensity in the arterial phase followed by inhomogeneous hypointensity (10.8%, 10) and inhomogeneous hyperintensity (1.1%, 1). In the delayed phase, the majority of the lesions (75.3%, 70) exhibited central hyperintensity with peripheral hypointensity followed by central inhomogeneous hypointensity with peripheral lower rim hypointensity (22.6%, 21) and inhomogeneous hypointensity (1.5%, 1). In the delayed phase, 90 (96.8%) lesions exhibited peripheral rim-like hypointensity with "target" appearances.

All of the 93 (100%) dominant masses were observable in the DW images. 80 (86.0%) lesions exhibited peripheral hyperintensity with central inhomogeneous hypointensity (39) or mixed signals (41), and 13 (14.0%) lesions exhibited inhomogeneous hyperintensity.

Enhancement patterns: Peripheral enhancement in the arterial phase followed by progressive centripetal enhancement in the portal venous and delayed phases was the most common enhancement pattern (86.0%, 80; **Figure 1**) followed by weak enhancement in the arteral phase and gradual enhancement in the subsequent phases (10.8%, 10; **Figure 2**), and 1 case (1.1%) of strong enhancement in the arterial phase and wash out in the portal venous and delayed phases.

Morphological features of the lesions: 44 cases (47.3%) of bile duct dilation were observed including 26 cases (59.0%, 26/44) of upstream bile duct dilation and 18 cases (41.0%, 18/44) of upstream and downstream bile duct dilatation. Capsule retraction and capsule bulging were observed in 28 (30.1%) and 7 cases (7.5%), respectively. Different numbers of satellite nodules were found in 39 cases (41.9%), and lymph node metastases were observed in 21 cases (22.6%). Additionally, vascular invsion was observed in 23 cases (24.7%).

Characteristics of the lesions on hepatobiliary phase (HBP) images: Regarding the lesion border evaluations, the highest subjective conspicuity ratings were observed on HBP images (median, 5; interquartile range, 4-5), and these ratings were significantly greater than those of the dynamic enhancement phases (median, 4; interquartile range 3-5). In the 39 cases in which satellite nodules were found, there were 2 cases (2/39) that satellite nodule was only found on HBP images but not in other enhancement phases. Peripheral rim-like hypointensity with central hyperintensity (91.4%, 85) was the most prevalent signal characteristic on HBP images (**Figures 1**, **3**) followed by 5 cases (5.4%) that exhibited inhomogeneous hypointensities, and 1 case (1.1%) that exhibited a high-low mixed signal intensity. Among the 80 cases of central hypointensity with peripheral hyperintensity in the arterial phase, the vast majority (97.5%, 78) exhibited central hyperintensity with peripheral rim-like hypointensity on HBP images. Regarding the remaining 2 cases (2.5%), one exhibited inhomogeneous hypointensity without peripheral hypointensity on HBP images, and the other exhibited a discontinuous hypointense rim in the periphery of the lesion. Among the 85 cases with central hyperintensity with peripheral hypointensity on HBP images, 50 cases (58.8%, 50/85) exhibited central hyperintensity with peripheral hypointensity in the delayed phase (**Table 2**).

Results of the quantitative analyses

A total of 93 lesions were measured in our study. 57 of these lesions (61.3%) were located in the left lobe of the liver, 26 (28.0%) were located in the right lobe of the liver, and 10 (10.7%) were located in the center. The average lesion diameter was 6.2 ± 2.5 cm (range: 2.2-12.3 cm). The percentage contrast enhancement relative to the normal liver parenchyma in the arterial phase, portal venous phase, delayed phase and HBP were 29.3%, 71.7%, 63.6%, and 57.2%, respectively. The majority of the lesions (91.4%, 85) exhibited the strongest enhancement in the portal venous phase. The enhancement percentage of all lesions in each phase were also calculated. The greatest enhancement occurred in the arterial phase in 8 cases (8.6%), in the venous phase in 13 cases (14.0%), in the delayed phase in 47 cases (50.5%), and on HBP in 26 cases (28.0%). The average ADC value of all of the lesions was 0.9×10^{-3} mm^2/s ± 0.33×10^{-3} mm^2/s (range:

0.65×10^{-3} mm^2/s to 1.42×10^{-3} mm^2/s), and the average ADC value of the normal liver tissue was 1.48×10^{-3} $mm^2/s \pm 0.19\times10^{-3}$ mm^2/s.

The 93 lesions were divided into 6 subgroups according to the morphological and histopathological characteristics of the lesions, and the percentages of contrast enhancement on HBP images and ADC values were also compared. The moderately differentiated lesions (48.2% ± 15.6%) exhibited a significantly higher percentage of enhancement on HBP images than the poorly differentiated lesions (35.5% ± 18.9%; *P*=0.028). Additionally, the lesions with lymph node metastasis (33.7% ± 19.6%) exhibited a lower enhancement percentage on HBP images than the lesions without lymph node metastasis (47.6% ± 18.8%; *P*=0.022). No significant between-subgroup differences were found in terms of satellite nodules or bile duct invasion, serosal invasion, and vascular invasion of the lesions. Moreover, the average ADC values of the moderately differentiated lesions (0.98×10^{-3} $mm^2/s \pm 0.22\times10^{-3}$ mm^2/s) were greater than those of the poorly differentiated lesions (0.75×10^{-3} $mm^2/s \pm 0.18\times10^{-3}$ mm^2/s; *P*=0.033). The other 5 subgroups did not exhibit significant differences (**Table 3**).

Discussion

Previous research on the use of Gd-BOPTA-enhanced MR to evaluate IMCs is rare [17-19], and we are the first to extensively report the imaging features of IMC on Gd-BOPTA-enhanced MR imaging. In our study, peripheral rim enhancement in the arterial phase followed by progressive centripetal enhancement in the portal venous and delayed phases was the most prevalent enhancement pattern of the IMCs (86.0%, 80), which is consistent with the results obtained in previous CT and MR studies involving conventional extracellular contrast materials [20-24], and this enhancement pattern was also consistent with previous results obtained with the liver-specific contrast agents Gd-BOPTA and Gd-EOB-DTPA [19, 25-27]. Pathologically, the typical enhancement pattern of IMCs is caused by the growth of a large number of active viable tumor cells and plentiful tumor vessels in the peripheral area of the tumor, which cause the peripheral enhancement and hyperintensity, and a large amount of fibrous tissue in the central area of tumor causes the centripetal progressive enhancement on MR images [25]. 10 cases (10.8%) in our study exhibited peripheral weak enhancement in the arterial phase and progressive enhancement in the portal venous and delayed phases, which might have been due to relative hypovascularity in the peripheral areas of the tumors.

Notably, in our study, one case exhibited a pattern of marked enhancement in the arterial phase, and the contrast material washed out in the portal venous and delayed phases, and this pattern is very similar to that of HCC. Previous studies have shown that this atypical pattern may be due to the presence of a large number of tumor vessels in the fibrotic stroma [28]. Although such enhancement patterns are rare in IMCs, they should be given proper attention because it is very difficult to differentiate hypervascular IMCs from HCCs.

In the arterial phase, the majority of the lesions (80, 86.0%) exhibited central hypointensity with peripheral hyperintensity, and 74 of 80 (74/80, 92.5%) cases exhibited central hyperintensity with peripheral hypointensity on HBP images. Due to the strong growth of tumor cells and the lack of normal liver cells in the periphery of the tumors, Gd-BOPTA cannot be taken up by tumor cells on HBP images, and the tumor cells thus exhibited hypointensity.

In our study, 70 lesions (75.3%) exhibited central hyperintensity with peripheral hypointensity in delayed phase, and 21 lesions (22.6%) exhibited central inhomogeneous hypointensity with peripheral lower rim hypointensity. Previous studies have researched the characteristics of this peripheral rim-like hypointensity in the delayed phase, which has been defined as “target appearance” [18]. In the presence of abundant blood vessels and tumor cells in the periphery, the contrast material is released in the delayed phase and exhibits hypointensity. Central hyperintensity in the delayed phase results from larger extracellular spaces in the central area, and contrast material gradually infiltrates the fiber matrix of the lesions, which causes the retention of contrast material and subsequent hyperintensity [29]. For these lesions with central inhomogeneous hypointensities, such signals in the center may be due to the larger areas of necrosis within the lesions or to the slower entry of the contrast material due to the dense fibrous tissue within the lesions. However, these areas of central inhomogeneous hypointensity in the delayed phase

were found to exhibit a trend of gradual filling with respect to the arterial and portal venous phases, and the areas of inhomogeneous hypointensity (with the exception of the necrotic areas) in the delayed phase were hyperintense on HBP images (**Figure 3**).

In our study, 85 lesions (91.4%) exhibited central hyperintensity and peripheral hypointensity on HBP, similar to the target appearance, which is consistent with the results obtained with previous studies of Gd-BOPTA-enhanced MR images [18, 19, 30]. Peripheral hypointensity results from the lack of normal hepatocytes in the periphery of the IMC, and central hyperintensity results from contrast material retention in the central fibrotic stroma. Among the 85 cases with typical imaging features on HBP images, 46 cases (46/85, 54.1%) exhibited target appearance with central hyperintensity and peripheral hypointensity in the delayed phase. Lacomis et al. [21] believe that the retention of contrast material in the delayed phase occurs primarily in well-differentiated IMCs as opposed to poorly differentiated IMCs. Notably, on the Gd-BOPTA-enhanced MR images, the target appearances of IMCs on HBP images were different from the appearances on Gd-EOB-DTPA-enhanced images. Most of the IMCs exhibit homogeneous or inhomogeneous hypointensities on HBP on Gd-EOB-DTPA-enhanced images [25, 27]. Compared with Gd-BOPTA-enhanced images, this finding might because of the more rapid hepatocellular uptake of Gd-EOB-DTPA on HBP, and it results in greater enhancement of the liver parenchyma [31, 32], which results in relative lesion hypointensity. Of course, on Gd-BOPTA-enhanced images, the typical target appearance on HBP images generally suggests the diagnosis of IMC, but we should note that this is not a specific feature of IMCs on HBP, it is also common to metastatic adenocarcinoma [30].

In our study, we evaluated the conspicuities of IMCs on MR images. We found that the tumors exhibited the greatest conspicuity on HBP images, that was because that the degree of enhancement of the liver parenchyma on HBP was not significantly decreased, and the peripheral rim hypointensity provided good contrast between the lesion and the adjacent liver parenchyma. Therefore, the lesions were more clearly illustrated. The conspicuities of IMCs on Gd-EOB-DTPA-enhanced images has previously been studied [25, 27], and the same conclusion was obtained. Because the IMCs exhibited the greatest conspicuity on HBP images, this phase should be used to better depict the border of the mass better and observe its delineation to aid the surgeon's operative planning. Satellite nodules are commonly found in IMCs [22, 23]. Of the 93 cases in our study, 39 cases (41.9%) were found to have satellite nodules around the tumors. Due to the high conspicuity on HBP, we observed satellite nodule near the lesion on HBP images in 2 cases (2/39, 5.1%), and these 2 satellite nodules were not observed on unenhanced T1WI, T2WI and dynamic enhancement phase images. With the exception of the two cases mentioned above, the satellite nodules of the other 26 cases were observable in each phase. Satellite nodules around IMCs are generally considered indicators of poor prognoses [22, 23].

We also evaluated the degree of enhancement of IMCs on HBP images. We found that the degree of enhancement of the moderately differentiated IMCs (48.2% ± 15.6%) was greater than that of the poorly differentiated IMCs (35.5% ± 18.9%) on HBP, and the degree of enhancement of the IMCs without lymph node metastases (47.6% ± 18.8%) were greater than those with lymph node metastases (33.7% ± 19.6%). Few studies have examined the degrees of enhancement of lesions on HBP images [25]. Some researchers believe that the degree of enhancement is related to the amount of fibrous stroma [33], and some scholars have suggested that well-differentiated IMCs are more likely to exhibit contrast material retention in delayed phase [21] and thus that the relative degree of enhancement of well-differentiated IMCs is higher. Poor differentiation and lymph node metastasis have both been related to poor prognoses [34, 35].

DWI has been proven to be an important functional imaging sequence due to its ability to differentiate tissues based on cellular density and architectural changes. Currently DW imaging is a standard MR protocol for detecting and characterizing focal liver disease [36, 37]. Some studies have reported the characteristics of focal liver lesions on DW images [38, 39], but few reports the features of intrahepatic cholan-

giocarcinomas, particularly IMCs, on DW images [40, 41]. In the present study, we analyzed the characteristics of 93 lesions on DW images and measured the ADC values of both the tumors and adjacent liver parenchyma. All of the lesions were observable on DW images, and most of the lesions (80, 86.0%) exhibited peripheral hyperintensity with central inhomogeneous hypointensity or mixed signal. Park et al. [41] reported that the target sign of small IMCs (≤3 cm in diameter) on DW images is a reliable imaging feature for the differentiation of IMCs from small HCCs. However, the target appearance of larger IMCs (>3 cm) on DW images has not yet been reported. The ADC value is a measure of water mobility that can be calculated based on ROIs in DW images. In ADC measurements the value of b is a very important source of variability. Zhang et al. [42] reported that higher b values are associated with more accurate ADC values. Cui et al. [43] believed that lesions exhibit higher CNR, SIR and SNR values at b=800 sec/mm^2, which facilitates the clear identification of masses. Therefore, we select a b value of 800 sec/mm^2 for this study. The ADC values of the tumors we measured (0.9×10^{-3} mm^2/s ± 0.33×10^{-3} mm^2/s) were significantly lower than those of the surrounding normal liver tissue (1.48×10^{-3} mm^2/s ± 0.19×10^{-3}mm^2/s), which is consistent with the results of a previous study that found that the ADC values of malignancies are lower than those of the liver parenchyma [44]. We also been observed that the ADC values of poorly differentiated tumors (0.75×10^{-3} mm^2/s ± 0.18×10^{-3} mm^2/s) were lower than those of moderately differentiated tumors (0.98×10^{-3} mm^2/s ± 0.22×10^{-3} mm^2/s) because as the degree of malignancy of the lesion increases, high levels of cell proliferation lead to increased cell density and increased intracellular macromolecular organelle densities in poorly differentiated tumors. Thus, the extracellular space is narrowed, which restricts the mobility of water molecules and results in decreases in ADC values [43]. Because poorly differentiated tumors lead to poor prognoses, the ADC values can be measured on MR images to predict the degree of tumor differentiation prior to surgery to make better therapeutic plans and improve prognoses.

Our study also has some limitations. First, this was a retrospective study, and patient selection bias might have been present. Second, we did not directly compare the enhanced MR features of IMCs that resulted from conventional extracellular contrast materials (such as Gd-DTPA) and Gd-BOPTA. Third, we did not directly compare IMCs and other tumors of the liver (e.g., HCC). Fourth, because the lesions in our study were all treated with surgical resection, and multiple distant metastases from the liver was a contraindication for surgery, we did not evaluate the features of the intrahepatic metastases of IMC.

In conclusion, we evaluated the features of IMCs on Gd-BOPTA-enhanced MR images and found that the typical enhancement pattern of IMCs involved a peripheral rim enhancement in the arterial phase and a gradual enhancement in the portal venous and delayed phases. The majority of IMCs exhibited target appearances involving a peripheral rim-like hypointensity on the delayed phase and HBP images, and this target appearance was also observed on DW images, which also included the characteristic of peripheral rim-like hyperintensity. On HBP images, the majority of the lesions exhibited central hyperintensity with peripheral rim-like hypointensity. Moreover, the IMCs exhibited greater conspicuities on HBP, which may help to improve surgical treatment by providing better delineation of tumors and satellite nodules. Additionally, we found that the degrees of enhancement of the moderately differentiated lesions and the lesions without lymph node metastasis were be higher than those of the poorly differentiated lesions and the lesions with lymph node metastases on HBP images. The ADC values of the poorly differentiated IMCs were lower than those of the moderately differentiated tumors, and this difference is significant for the prediction of the degree of tumor differentiation prior to surgery to improve the therapeutic plan.

Disclosure of conflict of interest

None.

Abbreviations

IMC, intrahepatic mass-forming cholangiogcarcinoma; HBP, hepatobiliary phase; DWI, diffusion-weighted image; ADC, apparent diffusion coefficient; HCC, hepatocellular carcinoma; US, ultrasound; CT, computerized tomography; MR, magnetic resonance; HCC-CC, combined hepatocellular and cholangiocarcinomas; PACS, picture archiving and communication system

workstation; SI, signal intensity; ROI, regions of interest; SD, standard deviation.

Address correspondence to: Jianjun Xiu, Department of Radiology, Shandong Provincial Hospital Affiliated to Shandong University, No. 324 Jingwu Road, Jinan 250021, China. Tel: +86-0531-68773658; E-mail: xjjxrx@sina.com

References

[1] Nakanuma Y, Sato Y, Harada K, Sasaki M, Xu J, Ikeda H. Pathological classification of intrahepatic cholangiocarcinoma based on a new concept. World J Hepatol 2010; 2: 419-427.

[2] Khan SA, Thomas HC, Davidson BR, Taylor-Robinson SD. Cholangiocarcinoma. Lancet 2005; 366: 1303-1314.

[3] Vilgrain V. Staging cholangiocarcinoma by imaging studies. HPB (Oxford) 2008; 10: 106-109.

[4] Nakeeb A, Pitt HA, Sohn TA, Coleman J, Abrams RA, Piantadosi S, Hruban RH, Lillemoe KD, Yeo CJ, Cameron JL. Cholangiocarcinoma. A spectrum of intrahepatic, perihilar, and distal tumors. Ann Surg 1996; 224: 463-473; discussion 473-465.

[5] Lim JH. Cholangiocarcinoma: morphologic classification according to growth pattern and imaging findings. AJR Am J Roentgenol 2003; 181: 819-827.

[6] Slattery JM, Sahani DV. What is the current state-of-the-art imaging for detection and staging of cholangiocarcinoma? Oncologist 2006; 11: 913-922.

[7] Tanimoto A, Lee JM, Murakami T, Huppertz A, Kudo M, Grazioli L. Consensus report of the 2nd International Forum for Liver MRI. Eur Radiol 2009; 19 Suppl 5: S975-S989.

[8] Balci NC, Semelka RC. Contrast agents for MR imaging of the liver. Radiol Clin North Am 2005; 43: 887-898, viii.

[9] Schneider G, Reimer P, Mamann A, Kirchin MA, Morana G, Grazioli L. Contrast agents in abdominal imaging: current and future directions. Top Magn Reson Imaging 2005; 16: 107-124.

[10] Hamm B, Staks T, Muhler A, Bollow M, Taupitz M, Frenzel T, Wolf KJ, Weinmann HJ, Lange L. Phase I clinical evaluation of Gd-EOB-DTPA as a hepatobiliary MR contrast agent: safety, pharmacokinetics, and MR imaging. Radiology 1995; 195: 785-792.

[11] Cavagna FM, Maggioni F, Castelli PM, Dapra M, Imperatori LG, Lorusso V, Jenkins BG. Gadolinium chelates with weak binding to serum proteins. A new class of high-efficiency, general purpose contrast agents for magnetic resonance imaging. Invest Radiol 1997; 32: 780-796.

[12] Spinazzi A, Lorusso V, Pirovano G, Kirchin M. Safety, tolerance, biodistribution, and MR imaging enhancement of the liver with gadobenate dimeglumine: results of clinical pharmacologic and pilot imaging studies in nonpatient and patient volunteers. Acad Radiol 1999; 6: 282-291.

[13] Brismar TB, Dahlstrom N, Edsborg N, Persson A, Smedby O, Albiin N. Liver vessel enhancement by Gd-BOPTA and Gd-EOB-DTPA: a comparison in healthy volunteers. Acta Radiol 2009; 50: 709-715.

[14] Dahlqvist Leinhard O, Dahlstrom N, Kihlberg J, Sandstrom P, Brismar TB, Smedby O, Lundberg P. Quantifying differences in hepatic uptake of the liver specific contrast agents Gd-EOB-DTPA and Gd-BOPTA: a pilot study. Eur Radiol 2012; 22: 642-653.

[15] Hecht EM, Israel GM, Krinsky GA, Hahn WY, Kim DC, Belitskaya-Levy I, Lee VS. Renal masses: quantitative analysis of enhancement with signal intensity measurements versus qualitative analysis of enhancement with image subtraction for diagnosing malignancy at MR imaging. Radiology 2004; 232: 373-378.

[16] Landis JR, Koch GG. The measurement of observer agreement for categorical data. Biometrics 1977; 33: 159-174.

[17] Jeon TY, Kim SH, Lee WJ, Lim HK. The value of gadobenate dimeglumine-enhanced hepatobiliary-phase MR imaging for the differentiation of scirrhous hepatocellular carcinoma and cholangiocarcinoma with or without hepatocellular carcinoma. Abdom Imaging 2010; 35: 337-345.

[18] Mamone G, Marrone G, Caruso S, Carollo V, Gentile G, Crino F, Milazzo M, Luca A. Intrahepatic mass-forming cholangiocarcinoma: enhancement pattern on Gd-BOPTA-MRI with emphasis of hepatobiliary phase. Abdom Imaging 2015; 40: 2313-2322.

[19] Quaia E, Angileri R, Arban F, Gennari AG, Cova MA. Predictors of intrahepatic cholangiocarcinoma in cirrhotic patients scanned by gadobenate dimeglumine-enhanced magnetic resonance imaging: diagnostic accuracy and confidence. Clin Imaging 2015; 39: 1032-1038.

[20] Maetani Y, Itoh K, Watanabe C, Shibata T, Ametani F, Yamabe H, Konishi J. MR imaging of intrahepatic cholangiocarcinoma with pathologic correlation. AJR Am J Roentgenol 2001; 176: 1499-1507.

[21] Lacomis JM, Baron RL, Oliver JH 3rd, Nalesnik MA, Federle MP. Cholangiocarcinoma: delayed CT contrast enhancement patterns. Radiology 1997; 203: 98-104.

[22] Zhang Y, Uchida M, Abe T, Nishimura H, Hayabuchi N, Nakashima Y. Intrahepatic peripheral cholangiocarcinoma: comparison of

dynamic CT and dynamic MRI. J Comput Assist Tomogr 1999; 23: 670-677.
[23] Vanderveen KA, Hussain HK. Magnetic resonance imaging of cholangiocarcinoma. Cancer Imaging 2004; 4: 104-115.
[24] Soyer P, Bluemke DA, Reichle R, Calhoun PS, Bliss DF, Scherrer A, Fishman EK. Imaging of intrahepatic cholangiocarcinoma: 1. Peripheral cholangiocarcinoma. AJR Am J Roentgenol 1995; 165: 1427-1431.
[25] Kang Y, Lee JM, Kim SH, Han JK, Choi BI. Intrahepatic mass-forming cholangiocarcinoma: enhancement patterns on gadoxetic acid-enhanced MR images. Radiology 2012; 264: 751-760.
[26] Hwang J, Kim YK, Park MJ, Lee MH, Kim SH, Lee WJ, Rhim HC. Differentiating combined hepatocellular and cholangiocarcinoma from mass-forming intrahepatic cholangiocarcinoma using gadoxetic acid-enhanced MRI. J Magn Reson Imaging 2012; 36: 881-889.
[27] Peporte AR, Sommer WH, Nikolaou K, Reiser MF, Zech CJ. Imaging features of intrahepatic cholangiocarcinoma in Gd-EOB-DTPA-enhanced MRI. Eur J Radiol 2013; 82: e101-e106.
[28] Chung YE, Kim MJ, Park YN, Choi JY, Pyo JY, Kim YC, Cho HJ, Kim KA, Choi SY. Varying appearances of cholangiocarcinoma: radiologic-pathologic correlation. Radiographics 2009; 29: 683-700.
[29] Murakami T, Nakamura H, Tsuda K, Ishida T, Tomoda K, Hori S, Monden M, Kanai T, Wakasa K, Sakurai M, et al. Contrast-enhanced MR imaging of intrahepatic cholangiocarcinoma: pathologic correlation study. J Magn Reson Imaging 1995; 5: 165-170.
[30] Kim YK, Lee JM, Kim CS. Gadobenate dimeglumine-enhanced liver MR imaging: value of dynamic and delayed imaging for the characterization and detection of focal liver lesions. Eur Radiol 2004; 14: 5-13.
[31] Filippone A, Blakeborough A, Breuer J, Grazioli L, Gschwend S, Hammerstingl R, Heinz-Peer G, Kittner T, Laghi A, Leen E, Lencioni R, Lucidarme O, Remplik P, Robinson PJ, Ruehm SG, Schaefer F, Stoupis C, Tombach B, Valette PJ, Zech CJ, Huppertz A. Enhancement of liver parenchyma after injection of hepatocyte-specific MRI contrast media: a comparison of gadoxetic acid and gadobenate dimeglumine. J Magn Reson Imaging 2010; 31: 356-364.
[32] Yamada A, Hara T, Li F, Fujinaga Y, Ueda K, Kadoya M, Doi K. Quantitative evaluation of liver function with use of gadoxetate disodium-enhanced MR imaging. Radiology 2011; 260: 727-733.
[33] Asayama Y, Yoshimitsu K, Irie H, Tajima T, Nishie A, Hirakawa M, Nakayama T, Kakihara D, Taketomi A, Aishima S, Honda H. Delayed-phase dynamic CT enhancement as a prognostic factor for mass-forming intrahepatic cholangiocarcinoma. Radiology 2006; 238: 150-155.
[34] DeOliveira ML, Cunningham SC, Cameron JL, Kamangar F, Winter JM, Lillemoe KD, Choti MA, Yeo CJ, Schulick RD. Cholangiocarcinoma: thirty-one-year experience with 564 patients at a single institution. Ann Surg 2007; 245: 755-762.
[35] Nakagohri T, Kinoshita T, Konishi M, Takahashi S, Gotohda N. Surgical outcome and prognostic factors in intrahepatic cholangiocarcinoma. World J Surg 2008; 32: 2675-2680.
[36] Heijmen L, Verstappen MC, Ter Voert EE, Punt CJ, Oyen WJ, de Geus-Oei LF, Hermans JJ, Heerschap A, van Laarhoven HW. Tumour response prediction by diffusion-weighted MR imaging: ready for clinical use? Crit Rev Oncol Hematol 2012; 83: 194-207.
[37] Koh DM, Collins DJ. Diffusion-weighted MRI in the body: applications and challenges in oncology. AJR Am J Roentgenol 2007; 188: 1622-1635.
[38] Dale BM, Braithwaite AC, Boll DT, Merkle EM. Field strength and diffusion encoding technique affect the apparent diffusion coefficient measurements in diffusion-weighted imaging of the abdomen. Invest Radiol 2010; 45: 104-108.
[39] Baltzer PA, Schelhorn J, Benndorf M, Dietzel M, Kaiser WA. Diagnosis of focal liver lesions suspected of metastases by diffusion-weighted imaging (DWI): systematic comparison favors free-breathing technique. Clin Imaging 2013; 37: 97-103.
[40] Fattach HE, Dohan A, Guerrache Y, Dautry R, Boudiaf M, Hoeffel C, Soyer P. Intrahepatic and hilar mass-forming cholangiocarcinoma: qualitative and quantitative evaluation with diffusion-weighted MR imaging. Eur J Radiol 2015; 84: 1444-1451.
[41] Park HJ, Kim YK, Park MJ, Lee WJ. Small intrahepatic mass-forming cholangiocarcinoma: target sign on diffusion-weighted imaging for differentiation from hepatocellular carcinoma. Abdom Imaging 2013; 38: 793-801.
[42] Zhang JL, Sigmund EE, Chandarana H, Rusinek H, Chen Q, Vivier PH, Taouli B, Lee VS. Variability of renal apparent diffusion coefficients: limitations of the monoexponential model for diffusion quantification. Radiology 2010; 254: 783-792.
[43] Cui XY, Chen HW, Cai S, Bao J, Tang QF, Wu LY, Fang XM. Diffusion-weighted MR imaging for detection of extrahepatic cholangiocarcinoma. Eur J Radiol 2012; 81: 2961-2965.
[44] Taouli B. Diffusion-weighted MR imaging for liver lesion characterization: a critical look. Radiology 2012; 262: 378-380.